

Article

Not peer-reviewed version

---

# Cranial Neural Crest Specific Deletion of TNAP Causes Abnormal Chondrocyte Maturation and Deficient Cranial Base Growth

---

[Naoto Ohkura](#) , [Hwa Kyung Nam](#) , Fei Liu , [Nan Hatch](#) \*

Posted Date: 30 August 2023

doi: 10.20944/preprints202308.1993.v1

Keywords: tissue nonspecific alkaline phosphatase; hypophosphatasia; cranial neural crest; cranial base; synchondrosis; chondrocyte, phosphate, pyrophosphate



Preprints.org is a free multidiscipline platform providing preprint service that is dedicated to making early versions of research outputs permanently available and citable. Preprints posted at Preprints.org appear in Web of Science, Crossref, Google Scholar, Scilit, Europe PMC.

Copyright: This is an open access article distributed under the Creative Commons Attribution License which permits unrestricted use, distribution, and reproduction in any medium, provided the original work is properly cited.

## Article

# Cranial Neural Crest Specific Deletion of TNAP Causes Abnormal Chondrocyte Maturation and Deficient Cranial Base Growth

Naoto Ohkura <sup>1,2</sup>, Hwa Kyung Nam <sup>1</sup>, Fei Liu <sup>3</sup> and Nan Hatch <sup>1,\*</sup>

<sup>1</sup> Department of Orthodontics and Pediatric Dentistry, School of Dentistry, University of Michigan, Ann Arbor, MI, USA; nhatch@umich.edu

<sup>2</sup> Division of Cariology, Operative Dentistry and Endodontics, Department of Oral Health Science, Niigata University Graduate School of Medical and Dental Sciences, Niigata, Japan; ohkura@dent.niigata-u.ac.jp

<sup>3</sup> Department of Biomaterials Sciences and Prosthodontics, School of Dentistry, University of Michigan, Ann Arbor, MI, USA; feiliu@umich.edu

\* Correspondence: nhatch@umich.edu

**Abstract:** Bone growth plate abnormalities and skull shape defects are seen in hypophosphatasia, a heritable disorder in humans that occurs due to deficiency of Tissue Nonspecific Alkaline Phosphatase (TNAP, *Alpl*) enzyme activity. Abnormal development of the cranial base growth plates (synchondroses) and abnormal skull shapes have also been demonstrated in global TNAP<sup>-/-</sup> mice. To distinguish local vs. systemic effects of TNAP on skull development, we utilized P0-Cre to knockout TNAP only in cranial neural crest derived tissues using TNAP flox mice. Here we show that TNAP deficiency in cranial neural crest leads to skull shape defects and deficient growth of the intersphenoid synchondrosis (ISS). ISS chondrocyte abnormalities included increased proliferation in resting and proliferative zones with decreased apoptosis in hypertrophic zones. ColX expression is increased, indicative of premature differentiation in the absence of TNAP. Sox9 expression is increased in both resting and prehypertrophic zones of mutant mice. Expression of PTHrP and IHH were also increased. Finally, cranial base organ culture revealed that inorganic phosphate (P<sub>i</sub>) and pyrophosphate (PP<sub>i</sub>) have specific effects on cell signaling and phenotype changes in the ISS. Together, these results demonstrate that TNAP expression in growth plate chondrocytes is essential for normal development, and that the mechanism likely involves Sox9, PTHrP, IHH and PP<sub>i</sub>.

**Keywords:** tissue nonspecific alkaline phosphatase; hypophosphatasia; cranial neural crest; cranial base; synchondrosis; chondrocyte; phosphate; pyrophosphate

## 1. Introduction

Long bone growth occurs at specific locations known as growth plates, where chondrocytes undergo a well-regulated process of proliferation and differentiation to form cartilage, which is then replaced by bone via apoptosis of terminally differentiated hypertrophic chondrocytes, and invasion of blood vessels to provide bone cells for bone formation [1,2]. This endochondral bone growth process also occurs in the skull bones of the cranial base, upon which the brain sits. In contrast to long bones, the cartilagenous bones of the cranial base are bidirectional, with a central resting zone surrounded on both anterior and posterior sides by proliferating, prehypertrophic and hypertrophic zones [3,4]. Cranial base growth plates are known as synchondroses. The two primary synchondroses of the cranial base in mice derive from different embryonic origins. The speno-occipital synchondrosis (SOS) is primarily of paraxial mesoderm origin while the intersphenoid synchondrosis (ISS) is of cranial neural crest origin [3]. Abnormal development and premature fusion of cranial base synchondroses is associated with numerous genetic disorders leading to deficient anterior-posterior growth of the skull, associated skull shape defects, and malocclusion (teeth not fitting together appropriately).

Hypophosphatasia is a rare inherited disorder caused by inactivating mutations in the gene (*Alpl*) that encodes the enzyme tissue non-specific alkaline phosphatase (TNAP). One primary and

well-established function of TNAP is to hydrolyze inorganic pyrophosphate (PP<sub>i</sub>) into inorganic phosphate (P<sub>i</sub>) [5]. Because PP<sub>i</sub> inhibits matrix mineralization while P<sub>i</sub> serves as a substrate for hydroxyapatite formation, TNAP activity promotes bone mineralization [6]. Both humans and mice that are affected by TNAP deficiency exhibit skeletal hypomineralization [7–9]. The influence of TNAP on skeletal development is not limited to mineralization. Humans and mice affected by TNAP deficiency also exhibit abnormal growth plates [8,10].

We previously investigated skull phenotype changes in the global *Alpl*<sup>-/-</sup> mouse model of hypophosphatasia to better understand mechanisms leading to craniosynostosis (premature fusion of calvarial/skull cap bones leading to high intracranial pressure) in a disorder of bone hypomineralization. We found evidence of skull bone hypomineralization, craniosynostosis and an abnormal skulls shape, which are also seen in infantile hypophosphatasia [9,11]. We also found evidence of abnormal development of cranial base synchondroses in these mice [12]. TNAP is highly expressed in hypertrophic zone chondrocytes [8] and we found expansion of the hypertrophic zone in global *Alpl*<sup>-/-</sup> mice. Isolation of rib chondrocytes from *Alpl*<sup>-/-</sup> mice revealed a cell autonomous influence of TNAP deficiency on chondrocytes [13].

Overall, our analyses of global *Alpl*<sup>-/-</sup> mice indicated that TNAP influenced skull bones of cranial neural crest more than those of paraxial mesoderm origin [12,13]. In addition, global *Alpl*<sup>-/-</sup> mice are phenotypically normal at birth but rapidly decline in health, with most dying before or shortly after weaning. Therefore, here we investigated the impact of TNAP deletion specifically in tissues of cranial neural crest origin at early and later stages of postnatal development by crossing *P0-Cre* promoter expressing mice for cranial neural crest expression [14], with floxed *Alpl* mice.

Results demonstrate that deletion of TNAP in cranial neural crest does not cause craniosynostosis, but does cause abnormal development of the anterior (neural crest origin) but not posterior (mesoderm origin) cranial base, and an abnormal skull shape. *Alpl*<sup>fl/fl</sup>; *P0-Cre*<sup>+</sup> mice exhibit abnormal chondrocyte proliferation, maturation and apoptosis, as well as aberrant Sox9, PTHrP and IHH signaling in the intersphenoid synchondrosis ISS, as compared to *Alpl*<sup>fl/fl</sup> mice. Organ culture of wild type cranial base showed that P<sub>i</sub> and PP<sub>i</sub> regulate PTHrP and IHH signaling as well as chondrocyte maturation. Because P<sub>i</sub> and PP<sub>i</sub> levels are anticipated to be down and up respectively upon TNAP deletion, this latter data indicates that the chondrocyte changes in vivo may be mediated by locally increased PP<sub>i</sub>. Additionally, knockdown of TNAP by shRNA in the O9.1 neural crest cell line showed abnormalities in markers of differentiation and stemness, affirming a cell autonomous role for TNAP in neural crest cells.

## 2. Results

### 2.1. *Alpl* deletion by *P0-Cre* does not cause craniosynostosis but does lead to skull shape abnormalities.

*Alpl*<sup>fl/fl</sup>; *P0-Cre*<sup>+</sup> mice are born healthy and are similar in size and weight compared to control mice. By 35 days after birth, *Alpl*<sup>fl/fl</sup>; *P0-Cre*<sup>+</sup> mice remain healthy and viable but are diminished in size and weight compared to control mice (Figure 1A). An abnormal skull shape including midface deficiency is apparent in *Alpl*<sup>fl/fl</sup>; *P0-Cre*<sup>+</sup> mice by day 35 (Figure 1B). Skull linear measurements that are normalized for overall skull size reveal increased cranial height, decreased inner canthal distance, plus decreased nasal bone, nose, frontal bone and overall skull lengths (Figure 1C). Skull width and parietal bone length are not different between *Alpl*<sup>fl/fl</sup>; *P0-Cre*<sup>+</sup> and *Alpl*<sup>fl/fl</sup> mice. It is important to state that, although the individual linear distances between the genotypes appear small on the graph, this is because the measurements are presented as normalized to total skull length (nasale to opisthion). It is also important to note that these individual skull linear measurement differences add up to a grossly abnormal skull shape as seen in Figure 1B. Finally, no evidence of any type of craniosynostosis was found in any of the mice, regardless of genotype.

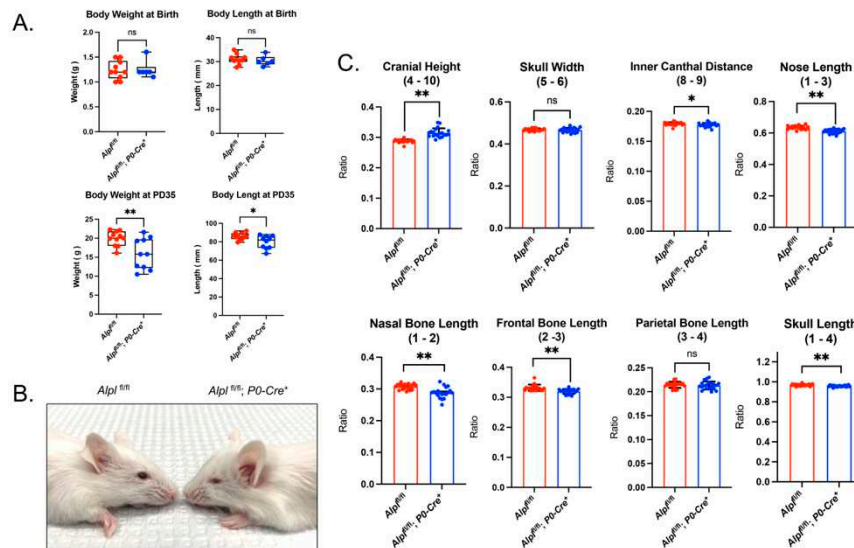


**Figure 1. Cranial neural crest cell-specific deletion of *Alpl* leads to skull shape defects.** (A) Body weight and body length in newborns is not different between genotypes. Body weight and body length are decreased in *Alpl<sup>fl/fl</sup>; P0-Cre<sup>+</sup>* as compared to *Alpl<sup>fl/fl</sup>* mice by postnatal day 35. (P35) (B) Representative 35 day-old mice are shown. Note midface hypoplasia evident in *Alpl<sup>fl/fl</sup>; P0-Cre<sup>+</sup>* but not in *Alpl<sup>fl/fl</sup>* mice. (C) Linear skull measurements normalized to a total skull length measurement to take into account differences in skull size between genotypes demonstrate craniofacial shape abnormalities in *Alpl<sup>fl/fl</sup>; P0-Cre<sup>+</sup>* mice at P35. As compared to *Alpl<sup>fl/fl</sup>* mice, *Alpl<sup>fl/fl</sup>; P0-Cre<sup>+</sup>* mice exhibit significantly increased cranial height, with significantly diminished inner canthal distance, nose length, nasal bone length, frontal bone length, and skull length. Skull width and parietal bone length are not different between genotypes. Overall, the skull shape of *Alpl<sup>fl/fl</sup>; P0-Cre<sup>+</sup>* mice is proportionally shorter in anterior-posterior length, and taller in height than the skull shape of *Alpl<sup>fl/fl</sup>* mice. \* $p < 0.05$ , \*\* $p < 0.01$  vs *Alpl<sup>fl/fl</sup>*. Red = *Alpl<sup>fl/fl</sup>*, Blue = *Alpl<sup>fl/fl</sup>; P0-Cre<sup>+</sup>*.  $n = 20$  per genotype.

## 2.2. P0-Cre *Alpl* deletion causes abnormal development of the anterior but not posterior cranial base

Nano-CT images revealed obvious abnormalities including fusions of the ISS but not the SOS (Figure 2A). 80% of *Alpl<sup>fl/fl</sup>; P0-Cre<sup>+</sup>* mice had partial or complete fusion of the ISS while no *Alpl<sup>fl/fl</sup>* mice had any evidence of fusion ( $p < 0.00001$ , Fisher exact test). Raw linear measurements of cranial base bones revealed an 11.4% decrease ( $p < 0.05$ ) in presphenoid bone length, a 9.6% decrease ( $p < 0.05$ ) in basisphenoid bone length, with no change in basioccipital bone length in *Alpl<sup>fl/fl</sup>; P0-Cre<sup>+</sup>* as compared to *Alpl<sup>fl/fl</sup>* mice. On the other hand, when each bone length was normalized for skull length (because the TNAP conditional knockout mice had smaller skulls than the control mice), there was a 10.0% decrease ( $p < 0.05$ ) in presphenoid bone length, a 7.7% decrease ( $p < 0.05$ ) in basisphenoid bone length, and a 4.0% increase ( $p < 0.05$ ) in basioccipital bone length in *Alpl<sup>fl/fl</sup>; P0-Cre<sup>+</sup>* as compared to *Alpl<sup>fl/fl</sup>* mice (Figure 2B).

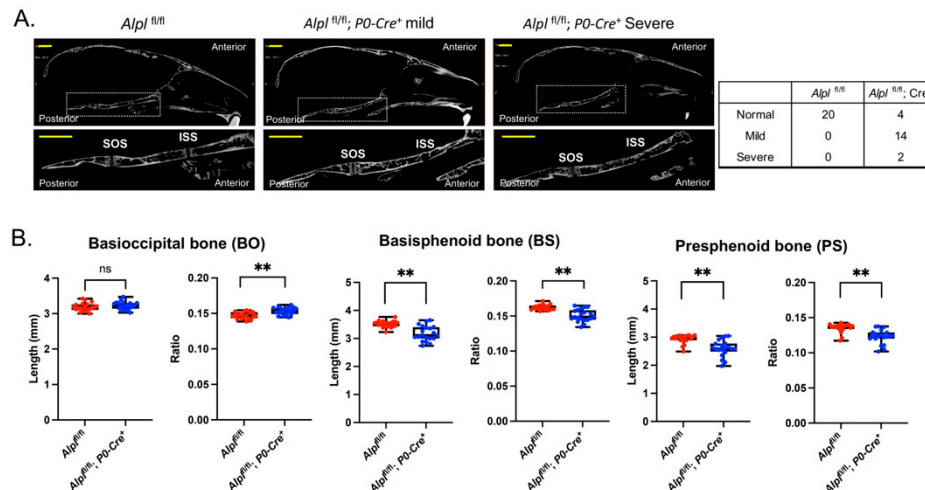


**Figure 2. Cranial neural crest cell-specific deletion of *Alpl* leads to cranial base defects.** (A) Nano-CT sagittal slice images of representative 35 day-old *Alpl*<sup>fl/fl</sup> and *Alpl*<sup>fl/fl</sup>; *P0-Cre*<sup>+</sup> skulls are shown. The dotted box and its magnified image show the cranial base. SOS = sphenoid-occipital synchondrosis; ISS = intersphenoid synchondrosis. Skulls of *Alpl*<sup>fl/fl</sup>; *P0-Cre*<sup>+</sup> mice showed partial to complete fusion of the ISS, which was not seen in any *Alpl*<sup>fl/fl</sup> mice. The SOS appeared normal in all mice regardless of genotype. (B) Nano-CT based measurements of cranial base bone lengths, and the lengths as normalized by total skull length to account for skull size differences, between genotypes are shown. Non-normalized basisphenoid and presphenoid bone lengths are diminished in *Alpl*<sup>fl/fl</sup>; *P0-Cre*<sup>+</sup> mice as compared to *Alpl*<sup>fl/fl</sup> mice. After normalization for total skull size, the basioccipital bone length is increased while basisphenoid and presphenoid bone lengths are decreased in *Alpl*<sup>fl/fl</sup>; *P0-Cre*<sup>+</sup> mice as compared to *Alpl*<sup>fl/fl</sup> mice. Yellow scale bars = 200  $\mu$ m. \*\**p* < 0.01 vs *Alpl*<sup>fl/fl</sup>. Red = *Alpl*<sup>fl/fl</sup>, Blue = *Alpl*<sup>fl/fl</sup>; *P0-Cre*<sup>+</sup>. n=20 per genotype.

To confirm specificity of TNAP knockdown in cranial neural crest derived tissues (e.g. the ISS and not the SOS), and to assess phenotypic changes within the TNAP deficient ISS, we performed histomorphometric analysis of stained sections from day 5 mice. Alkaline phosphatase staining for TNAP activity was strong in the hypertrophic and prehypertrophic zones of both the ISS and SOS of control *Alpl*<sup>fl/fl</sup> mice. In contrast, alkaline phosphatase staining was strong in the hypertrophic and prehypertrophic zones in the SOS but not the ISS of *Alpl*<sup>fl/fl</sup>; *P0-Cre*<sup>+</sup> mice (Figure 3A). Total ISS area was increased in *Alpl*<sup>fl/fl</sup>; *P0-Cre*<sup>+</sup> compared to *Alpl*<sup>fl/fl</sup> mice (Figure 3B). ISS chondrocyte zone widths as normalized for total ISS width demonstrated significantly increased width of the hypertrophic zone, and significantly decreased width of all other zones in *Alpl*<sup>fl/fl</sup>; *P0-Cre*<sup>+</sup> compared to *Alpl*<sup>fl/fl</sup> mice. While there appeared to be a greater area of Alcian Blue staining for cartilage matrix, there was no difference in staining per cell in any zones of the ISS in conditional TNAP knockout as compared to control mice (Figure 3C). No changes were found in SOS area, chondrocyte zone widths or alcian blue staining between *Alpl*<sup>fl/fl</sup>; *P0-Cre*<sup>+</sup> and *Alpl*<sup>fl/fl</sup> mice (data not shown).



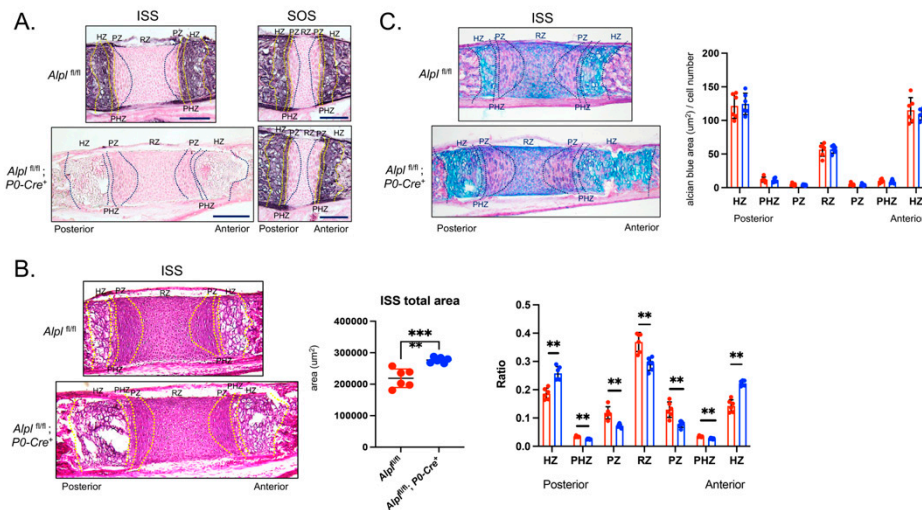


**Figure 3.** Cranial neural crest cell-targeted *Alpl* ablation leads to hypertrophic zone expansion in the intersphenoidal synchondrosis at postnatal day 5. (A) Alkaline phosphatase staining of the intersphenoid synchondrosis (ISS) and speno-occipital synchondrosis (SOS) demonstrates lack of TNAP enzyme activity in and around the ISS but not the SOS of *Alpl*<sup>fl/fl</sup>; *P0-Cre*<sup>+</sup> mice, indicative of cranial neural crest derived specific TNAP ablation. (B) Alcian blue staining of the ISS of *Alpl*<sup>fl/fl</sup> and *Alpl*<sup>fl/fl</sup>; *P0-Cre*<sup>+</sup> mice. More alcian blue staining is evident in ISS of *Alpl*<sup>fl/fl</sup>; *P0-Cre*<sup>+</sup> compared to *Alpl*<sup>fl/fl</sup> mice indicative of greater width of the hypertrophic zone, but not when normalized by cell number indicative of similar staining per cell. (C) Hematoxylin and Eosin staining showing the histology of the ISS with/without ablation of TNAP in cranial neural crest derived cells is shown. The total area of the ISS is greater in *Alpl*<sup>fl/fl</sup>; *P0-Cre*<sup>+</sup> as compared to *Alpl*<sup>fl/fl</sup> mice. Hypertrophic zone widths are significantly greater in *Alpl*<sup>fl/fl</sup>; *P0-Cre*<sup>+</sup> as compared to *Alpl*<sup>fl/fl</sup> mice, even after normalization to total ISS width (ratio). All other zones are significantly decreased after zone width normalization to total ISS width in *Alpl*<sup>fl/fl</sup>; *P0-Cre*<sup>+</sup> as compared to *Alpl*<sup>fl/fl</sup> mice. N=6 per genotype. Black scale bars = 200 μm. \*\*p<0.01, \*\*\*p<.005 between genotypes. Red = *Alpl*<sup>fl/fl</sup>, Blue = *Alpl*<sup>fl/fl</sup>; *P0-Cre*<sup>+</sup>. Zones were demarkated according to the following criteria. RZ: The nucleus is round. PZ: The nucleus is flat. PHZ: Adjacent to the PZ, and the cell shape is flattened and enlarged. HZ: The shape is greatly enlarged.

### 2.3. *P0-Cre Alpl* deletion increases chondrocyte proliferation and decreases apoptosis in the anterior cranial base synchondrosis (ISS).

Next, we performed Ki67 staining to quantify proliferating cells in the synchondroses of 5-day-old mice. Ki67 positive staining was mainly present in the resting zone (RZ) and proliferation zone (PZ) of the mice, regardless of genotype (Figure 4A). When comparing genotypes, Ki67 positive staining was significantly greater in the RZ and PZ of *Alpl*<sup>fl/fl</sup>; *P0-Cre*<sup>+</sup> mice compared to *Alpl*<sup>fl/fl</sup> ISS. No differences were noted between genotypes in the SOS (data not shown).

We next sought to determine if the *Alpl*<sup>fl/fl</sup>; *P0-Cre*<sup>+</sup> mice exhibited diminished synchondrosis chondrocyte apoptosis, as we had previously seen in global *Alpl*<sup>-/-</sup> mice [13]. While detection of apoptosis by either TUNEL or Annexin V staining (Annexin V staining not shown) revealed overall low levels of apoptosis in the ISS of 5-day-old mice; quantification revealed significantly decreased levels of apoptosis in both the posterior and anterior hypertrophic zones (HZ) in *Alpl*<sup>fl/fl</sup>; *P0-Cre*<sup>+</sup> as compared to *Alpl*<sup>fl/fl</sup> mice (Figure 4B). No differences were found between genotypes for the SOS (data not shown).

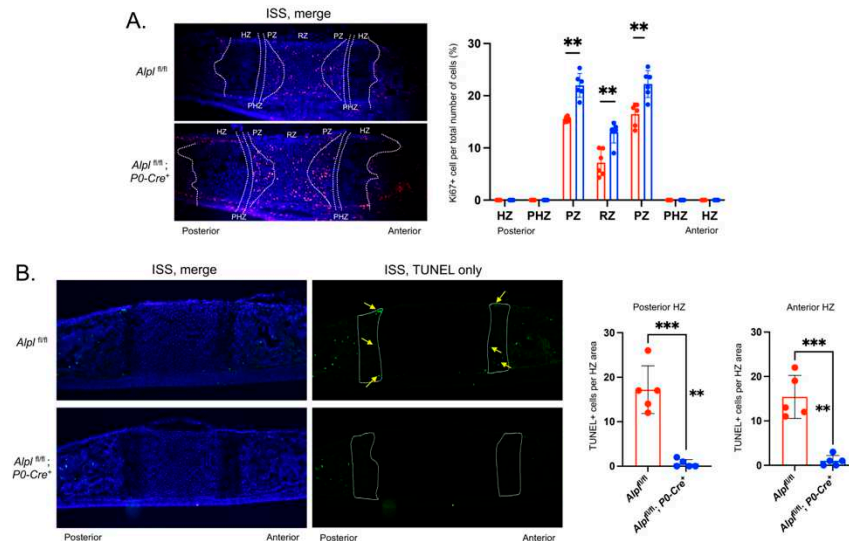


**Figure 4.** Cranial neural crest cell-targeted *Alpl* ablation leads to increased proliferation, and diminished apoptosis in the ISS at postnatal day 5. (A) Cells were immunostained for Ki67 (red) as a marker of proliferating cells and costained with nuclear dapi stain (blue). Merged stains are shown. Ki67+ cells relative to the total number of cells per chondrocyte zone were quantified and . (B) Cells were immunostained with TUNEL (green) to detect apoptotic DNA breaks and costained with nuclear dapi stain (blue). Merged and TUNEL only stains are shown. TUNEL+ cells relative to the total area of the anterior and posterior hypertrophic zones (HZ) were quantified (HZ outlined in yellow, yellow arrows point to TUNEL+ cells). N=6 per genotype. \*\*p<.01, \*\*\*p<.005 between genotypes. Red = *Alpl<sup>fl/fl</sup>*, Blue = *Alpl<sup>fl/fl</sup>; P0-Cre<sup>+</sup>*.

#### 2.4. *P0-Cre Alpl* deletion increased PTH related protein (PTHrP) and Indian Hedgehog (IHH) expression in the anterior cranial base synchondrosis (ISS).

Because interactive PTHrP-IHH signaling is known to coordinate diverse aspects of bone morphogenesis in long bone growth plates and cranial base synchondroses [15,16], we hypothesized that aberrant PTHrP-IHH signaling may underly the ISS abnormalities seen in *Alpl<sup>fl/fl</sup>; P0-Cre<sup>+</sup>* mice. Immunofluorescent staining for PTHrP in the ISS of 5-day-old mice showed increased PTHrP expression in the resting and hypertrophic zones of *Alpl<sup>fl/fl</sup>; P0-Cre<sup>+</sup>* as compared to *Alpl<sup>fl/fl</sup>* mice (Figure 5A). Immunofluorescent staining for IHH in the ISS of 5-day-old mice showed increased IHH expression in the prehypertrophic and hypertrophic zones of *Alpl<sup>fl/fl</sup>; P0-Cre<sup>+</sup>* as compared to *Alpl<sup>fl/fl</sup>* mice (Figure 5B). No differences were found between genotypes for the SOS (data not shown).

#### 2.5. *P0-Cre Alpl* deletion promotes premature chondrocyte differentiation in the anterior cranial base synchondrosis (ISS).

To determine if *Alpl* deletion by *P0-Cre* influences the maturation of chondrocytes in the cranial base synchondroses, we next performed immunofluorescent staining for Sex determining region Y-box 9 (Sox9), collagen II (Col II) and collagen X (Col X). Sox9 expression was higher in the resting and prehypertrophic zones of *Alpl<sup>fl/fl</sup>; P0-Cre<sup>+</sup>* as compared to *Alpl<sup>fl/fl</sup>* mice (Figure 5C). Col X expression was also significantly higher in *Alpl<sup>fl/fl</sup>; P0-Cre<sup>+</sup>* as compared to *Alpl<sup>fl/fl</sup>* mice in these same chondrocyte zones (Figure 5D). No differences were found between genotypes for Col II expression in the ISS (data not shown). No differences were found between genotypes for Sox9, Col II or Col X in the SOS (data not shown).

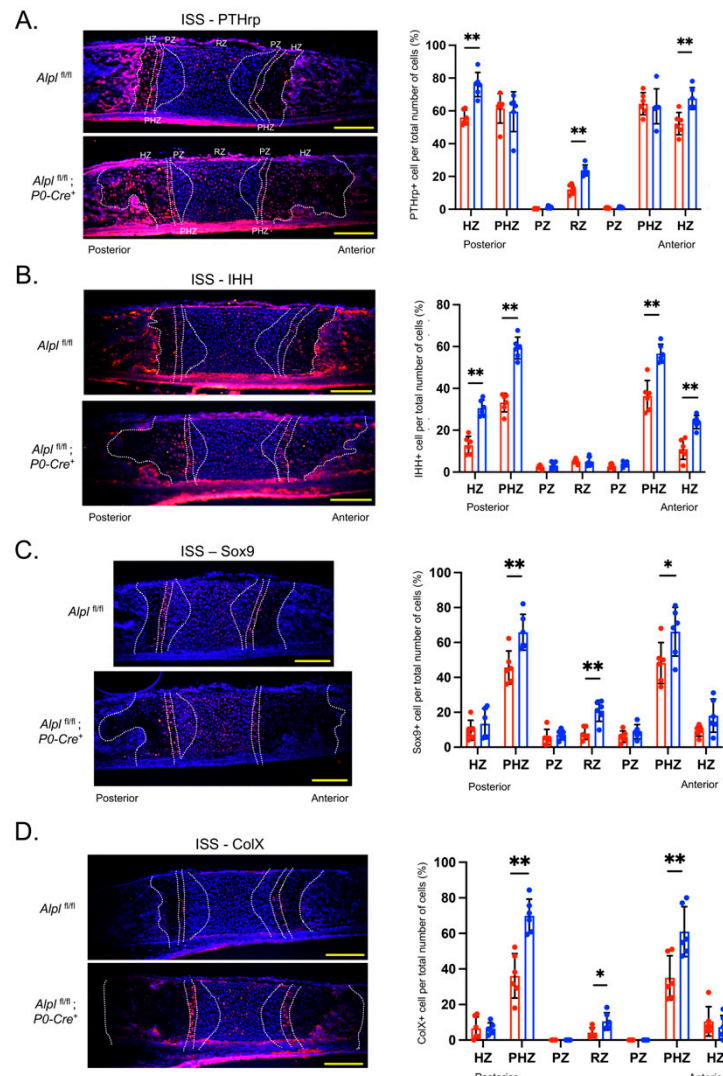


**Figure 5.** Cranial neural crest cell-targeted *Alpl* deletion alters expression of PTHrP, IHH, Sox9 and ColX in the ISS at postnatal day 5. (A) Cells were immunostained for PTHrP (red) and costained with nuclear dapi stain (blue), then quantified by cell count as normalized to total cell number per chondrocyte zone. (B) Cells were immunostained for PTHrP (red) and costained with nuclear dapi stain (blue), then quantified by cell count as normalized to total cell number per chondrocyte zone. (C) Cells were immunostained for Sox9 (red) and costained with nuclear dapi stain (blue), then quantified by cell count as normalized to total cell number per chondrocyte zone. (D) Cells were immunostained for ColX (red) and costained with nuclear dapi stain (blue), then quantified by cell count as normalized to total cell number per chondrocyte zone. n=6 per genotype. Yellow scale bars = 200  $\mu$ m. \*p<.05, \*\*p<.01 between genotypes. Red = *Alpl<sup>fl/fl</sup>*, Blue = *Alpl<sup>fl/fl</sup>; P0-Cre<sup>+</sup>* mice.

## 2.6. $PP_i$ and $P_i$ differentially regulate PTHrP-IHH signaling and chondrocyte maturation in cultured anterior cranial base.

A primary substrate for TNAP is  $PP_i$ , which is hydrolyzed to  $P_i$ . Therefore, TNAP deficiency leads to high  $PP_i$  and potentially low  $P_i$  levels, which prior studies have shown can influence gene expression and proliferation [17–19], in addition to influencing other cellular phenotypes including chondrocyte differentiation and apoptosis [20]. To determine if local changes in levels of  $PP_i$  and/or  $P_i$  could account for the changes seen in the ISS of *Alpl<sup>fl/fl</sup>; P0-Cre<sup>+</sup>* mice, we performed organ culture of newborn anterior cranial base isolated from wild type mice in  $P_i$  free media supplemented with/without  $PP_i$  or  $P_i$ . Tissues were stained with H&E or with a colorimetric substrate for TNAP to assess overall phenotype changes (Figure 6A). It was first noted that chondrocyte zones in the



anterior aspect of the ISS were difficult to distinguish, so quantifications were only performed in the posterior aspect of the ISS. In addition, due to difficulty in the ability to clearly distinguish all chondrocyte zones of the posterior ISS, histomorphometry was performed on combined resting and proliferating zones and on the hypertrophic zone. Quantification of stained sections demonstrated that culture with  $PP_i$  or  $P_i$  for five days increased ISS area. Culture with  $P_i$  but not  $PP_i$  increased the combined width of the resting and proliferative zones. Culture with either  $P_i$  and  $PP_i$  increased width of the hypertrophic zone, although  $PP_i$  did so significantly more than  $P_i$ .

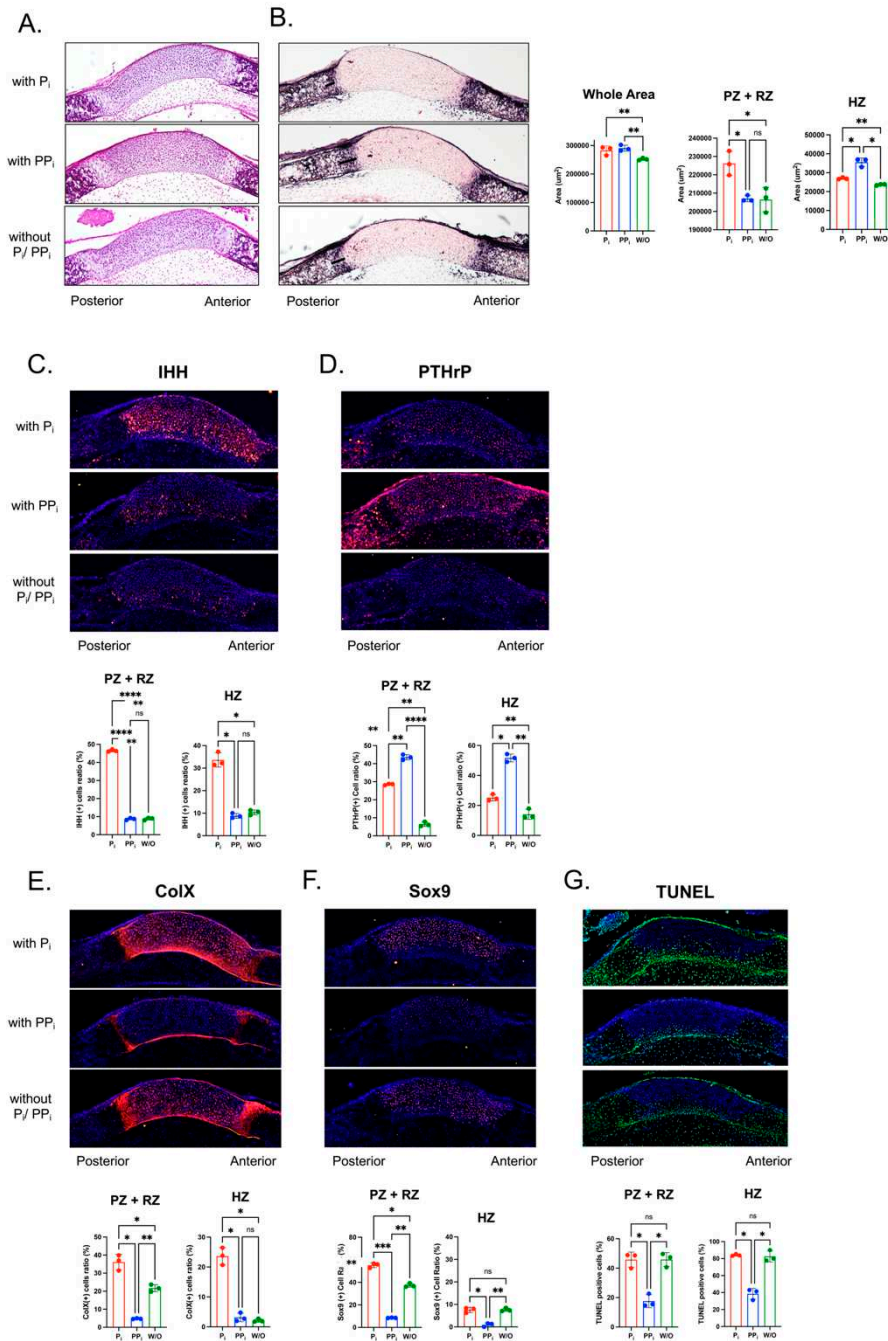


**Figure 6.** Inorganic phosphate ( $P_i$ ) and inorganic pyrophosphate ( $PP_i$ ) differentially alter cranial base signaling and differentiation in culture. Cranial base was dissected from newborn wild type mice and cultured in  $P_i$  free media that was supplemented with/without  $P_i$  or  $PP_i$  as indicated. Only the posterior HZ was measured because no bone mineralization was apparent on the anterior aspect of the ISS at birth. Moreover, the RZ and PZ could not be distinguished. Thus, we measured the zone of PZ+RZ and the posterior HZ. (A) Hematoxylin and eosin (H&E) staining and (B) alkaline phosphatase (AP) stains of cranial base sections after 5 days of culture with/without ( $P_i$ ) or ( $PP_i$ ). Stains were

quantified by counting immune-positive cells as divided by the total number of cells. (A) Hematoxylin and eosin (H&E) staining and (B) alkaline phosphatase (AP) stains of cranial base sections after 5 days of culture with/without ( $P_i$ ) or ( $PP_i$ ). Quantification of growth plate zones demonstrates that culture with  $P_i$  or  $PP_i$  increases overall width of the ISS, culture with  $P_i$  increases width of the resting (RZ) and proliferating zones (PZ), and culture with  $PP_i$  increases width of the hypertrophic zone (HZ). There were no significant differences in AP (alkaline phosphatase) activity between treatment groups. (C)  $PP_i$  and not  $P_i$  increases IHH signaling (red) in cultured ISS. (D)  $PP_i$  and, to a lesser extent,  $P_i$  increase PTHrP signaling (red) in cultured ISS. (E)  $P_i$  increases while  $PP_i$  decreases ColX expression (red) in cultured ISS. (F)  $P_i$  increases while  $PP_i$  decreases Sox9 expression (red) in cultured ISS. (G)  $PP_i$  decreases apoptosis as indicated by TUNEL staining (green) for DNA breaks. \* $p < 0.05$ , \*\* $p < 0.01$ , \*\*\* $p < 0.005$ , \*\*\*\* $p < 0.001$  between indicated treatment groups.

We next performed immunofluorescence staining to quantify levels of IHH and PTHrP (Figure 6B). Results show that  $P_i$  but not  $PP_i$  significantly increased IHH expression throughout the ISS and specifically as quantified in the combined resting and proliferative zones, and in the posterior hypertrophic zone. In contrast, culture with either  $P_i$  and  $PP_i$  increased PTHrP expression throughout the ISS and specifically as quantified in the combined resting and proliferative zones, and in the posterior hypertrophic zone, although  $PP_i$  did so to a significantly greater extent than  $P_i$ .

We quantified chondrocyte differentiation and apoptosis markers via immunofluorescence that were shown to be significantly altered in the ISS of *Alpl<sup>fl/fl</sup>;P0-Cre<sup>+</sup>* mice (Figure 6C). Staining and quantification revealed that  $P_i$  increased while  $PP_i$  decreased expression of Col X in the combined resting and proliferative zones, while  $P_i$  increased while  $PP_i$  had no effect on expression of Col X in the posterior hypertrophic zones. Similar results were found for Sox9 expression, except that  $P_i$  increased while  $PP_i$  decreased expression of Sox9 in the combined resting and proliferative zones, and in the posterior hypertrophic zone. TUNEL staining for apoptosis demonstrated that  $PP_i$  decreased while  $P_i$  had no impact on apoptosis levels in the combined resting and proliferative zones or the posterior hypertrophic zone.

## 2.7. *Alpl* deficient O9-1 cells influences the stemness and differentiation.

In the musculoskeletal field, TNAP is most widely known for its role in skeletal growth and mineralization. Yet, TNAP is also expressed in a wide variety of progenitor cells [21,22], including embryonic stem cells [23,24] and induced pluripotent stem cells [25]. To initiate an investigation of a potential TNAP influence on pluripotent neural crest cells, we knocked down expression of TNAP by stable transfection with *Alpl* (TNAP) shRNA in the O9.1 mouse neural crest cell line [26]. Transfection with *Alpl* but not with nontarget control shRNA significantly decreased alkaline phosphatase activity and expression of *Alpl* mRNA (Figure 7A). To determine if *Alpl* deletion influences chondrocyte differentiation, the cells were cultured in chondrogenic media then stained with alcian blue for cartilaginous matrix accumulation. O9.1 cells expressing *Alpl* shRNA exhibited significantly decreased staining for alcian blue when compared to cell expressing nontarget shRNA (Figure 7B). Real time PCR for mRNA changes revealed that O9.1 cells expressing *Alpl* shRNA expressed similar levels of the neural crest markers *AP-2a*, *Twist1* and *Snail1*, but expressed significantly lower levels of Sox9 mRNA as compared to the control cells (Figure 7C). Knockdown of TNAP in O9.1 cells decreased expression of the stem cell markers *Nestin* and *Sca-1*, but increased expression of *CD44*.

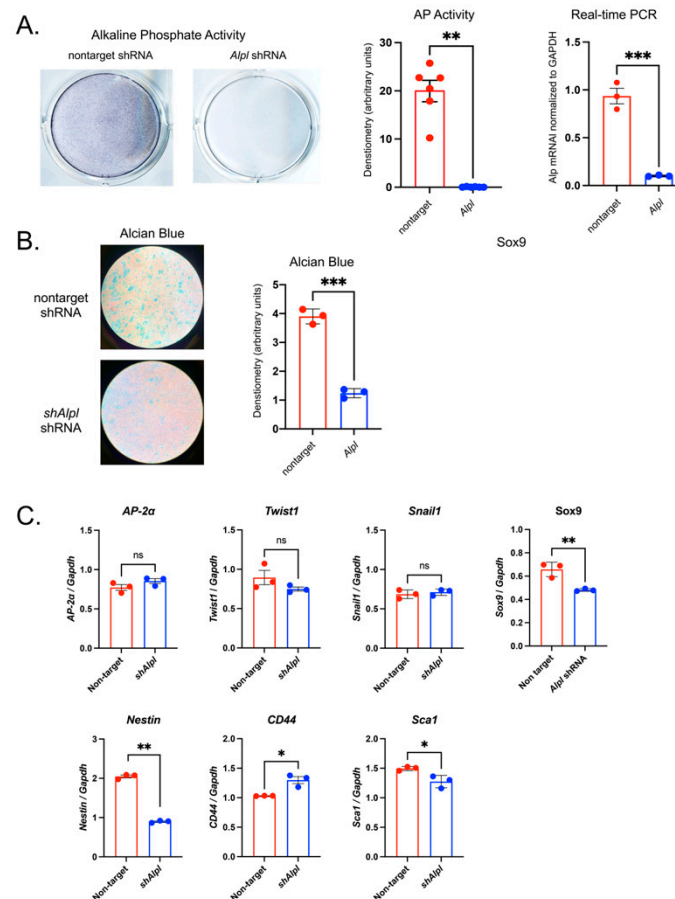


**Figure 7.** TNAP deficient O9-1 neural crest cells exhibit diminished proteoglycan accumulation plus aberrant expression of neural crest and stem cell markers. Cells were transduced with TNAP specific *Alpl* shRNA (*shAlpl*) or control nontarget shRNA. TNAP enzyme activity was visualized by incubation of cells with a colorimetric substrate and quantified by densitometry. mRNA levels were quantified by real time PCR and are presented as normalized to GAPDH. (A) TNAP activity and TNAP mRNA levels are significantly reduced in *shAlpl* O9-1 cells as compared to the control cells. (B) Cells were cultured under chondrocyte differentiation conditions for 7 days, stained with Alcian blue then quantified by densitometry. Alcian blue staining for proteoglycan accumulation was significantly diminished in *shAlpl* O9-1 cells as compared to the control cells. (C) Expression of Sox9 was diminished in TNAP deficient as compared to control cells, while other markers of neural crest were not different between genotype. Expression of Nestin was decreased while expression of CD44 and Sca1 were increased in TNAP deficient as compared to control cells. Red = non-target O9-1 cells, Blue = *shAlpl* O9-1 cells. \* $p < 0.05$ , \*\* $p < 0.01$  between genotype.

### 3. Discussion

The original goal of this study was to determine if deletion of TNAP in cranial neural crest cells would cause coronal craniosynostosis in mice. This idea was based upon our prior findings which showed that skull bones of cranial neural crest origin (e.g., facial bones, frontal bones) appeared to be more affected than those of mesoderm origin (e.g., parietal bones, occipital bones) and that coronal craniosynostosis occurred in approximately 1/3 of global *Alpl*<sup>-/-</sup> mice on mixed C57BL/6J-129/SvJ genetic background [12]. This level of incidence of craniosynostosis is similar to that reported to occur in infants and children with hypophosphatasia [11,27,28]. The coronal suture sits at a boundary between mesoderm derived parietal bones and neural crest derived frontal bones [29]. Early studies indicated that the coronal suture is mesoderm derived [30,31] while a more recent study showed that while the midsuture and parietal bone edge of the suture are mesoderm derived, the frontal bone edge of the suture is of cranial neural crest origin [32]. Therefore, coronal suture fusion could occur

via a neural crest cell autonomous or non-cell autonomous effect upon deletion of TNAP in cranial neural crest cells via *P0-Cre*. Craniosynostosis was not found in any of the *Alpl<sup>fl/fl</sup>;P0-Cre<sup>+</sup>* mice by 35 days postnatal, a time at which calvaria growth is essentially complete [33]. This data indicates that deletion of TNAP in paraxial mesoderm and/or deletion of TNAP in both cranial neural crest and paraxial mesoderm causes craniosynostosis in the *Alpl<sup>-/-</sup>* mouse model of hypophosphatasia, and likely in individuals affected by hypophosphatasia.

Despite lack of craniosynostosis, the *Alpl<sup>fl/fl</sup>; P0-Cre<sup>+</sup>* mice did exhibit an abnormal skull shape that was similar (increase in skull height; shorter anterior-posteriorly) and different (no increase in skull width) compared to the skull shape abnormalities seen in global *Alpl<sup>-/-</sup>* mice. Both global and cranial neural crest specific ablation of TNAP caused decreased anterior cranial base bone lengths and cranial base fusions, which could account for the decrease in total anterior-posterior skull length and compensating increase in skull height. It is also possible that the abnormal skull shape in TNAP deficient mice occurs due to direct effects of TNAP on cranial bone growth. Nasal bones are shorter in both *Alpl<sup>fl/fl</sup>;P0-Cre<sup>+</sup>* and *Alpl<sup>-/-</sup>* mice, and we previously reported diminished proliferation and a defect in cell cycle progression in TNAP deficient primary calvarial cells in culture [34,35]. TNAP is expressed in cranial bone rudiments several days prior to mineralization, but its function there is not yet established [36–38]. Future studies involving a more comprehensive and longitudinal analysis of cranial osteoprogenitor proliferation and cranial bone growth in *Alpl<sup>fl/fl</sup>;P0-Cre<sup>+</sup>* and/or *Alpl<sup>-/-</sup>* mice are needed to determine if cranial and/or facial bone growth differences impact the skull shape of TNAP deficient mice.

While we previously found dysregulated development of both the ISS and SOS in global *Alpl<sup>-/-</sup>* mice [13], in *Alpl<sup>fl/fl</sup>; P0-Cre<sup>+</sup>* mice only the ISS was abnormal (Figure 3A) because TNAP was ablated in the ISS but not in the SOS of these mice. Presphenoid and basisphenoid bones surrounding the ISS were shorter, and premature fusion of the ISS was found 80% of *Alpl<sup>fl/fl</sup>;P0-Cre<sup>+</sup>* as compared to *Alpl<sup>fl/fl</sup>* mice at 35 days postnatal. Histomorphometry of H&E stained 5-day-old ISS sections revealed significantly increased hypertrophic zone widths in the *Alpl<sup>fl/fl</sup>;P0-Cre<sup>+</sup>* mice, similar to that seen in global *Alpl<sup>-/-</sup>* mice [13]. This finding indicates that TNAP deficiency in local growth plate prehypertrophic and hypertrophic chondrocytes likely causes chondrocyte maturation defects leading to cranial base defects, because TNAP is normally expressed in these cells.

Hypertrophic zone chondrocyte apoptosis was decreased in *Alpl<sup>fl/fl</sup>;P0-Cre<sup>+</sup>* mice, accounting for the expanded hypertrophic zone width, and similar to that seen in global *Alpl<sup>fl/fl</sup>* mice [13], and in mouse models of hypophosphatemic rickets [39]. Proliferation was increased in the resting and proliferation zones of *Alpl<sup>fl/fl</sup>;P0-Cre<sup>+</sup>* mice, yet these zones were not increased in size compared to control mice, which could be explained if the proliferating cells of *Alpl<sup>fl/fl</sup>;P0-Cre<sup>+</sup>* mice were also enhanced in differentiation. Staining for Col X was increased in the *Alpl<sup>fl/fl</sup>;P0-Cre<sup>+</sup>* as compared to *Alpl<sup>fl/fl</sup>* mice, indicating that premature differentiation was occurring in addition to increased proliferation. Sox9 expression was up in both resting and hypertrophic zones. Sox9 is a master transcriptional regulator of chondrocytes that promotes chondrocyte proliferation and inhibits maturation in resting and proliferating zones, while promoting maturation and hypertrophy in prehypertrophic zones, via differential expression of co-transcription factors Sox5, Sox6, Runx2 and Mef2c [40–42]. Sox9 could therefore be mediating the ISS chondrocyte changes seen downstream of TNAP ablation in cranial neural crest cells. Col2 expression was not altered in *Alpl<sup>fl/fl</sup>;P0-Cre<sup>+</sup>* ISS (Supplemental Figure S2).

Indian Hedgehog (IHH) and Parathyroid Hormone Related Peptide (PTHrP) have long been known to play an essential role in chondrocyte proliferation and maturation in long bone growth growth plates [15,43,44]. The IHH-PTHrP feedback loop is also considered essential for cranial base growth plates [45,46]. PTHrP is secreted from resting zone chondrocytes to promote proliferation and inhibit chondrocyte maturation, while also inhibiting the production of IHH. More distant cells in the prehypertrophic and hypertrophic zones express IHH, which in turn promotes proliferation and differentiation, while also stimulating PTHrP expression to impact resting zone chondrocytes. Because this signaling feedback loop is considered essential for regulation of growth plates and subsequent endochondral bone growth, we investigated expression of IHH and PTHrP in the ISS of



*Alpl<sup>fl/fl</sup>;P0-Cre<sup>+</sup>* mice as compared to control mice. We found increased expression of IHH in prehypertrophic and hypertrophic zones, in addition to increased expression of PTHrP in hypertrophic and resting zones of *Alpl<sup>fl/fl</sup>;P0-Cre<sup>+</sup>* ISS. Because TNAP and IHH are normally expressed in prehypertrophic and hypertrophic zones, our data suggests that TNAP deficiency in these zones causes high IHH expression, in turn leading to ectopic expression of PTHrP in the hypertrophic zone plus increased PTHrP expression in the resting zone, where PTHrP is normally expressed.

Apoptosis of hypertrophic zone chondrocytes was previously shown to be stimulated by inorganic phosphate ( $P_i$ ) and inhibited by inorganic pyrophosphate ( $PP_i$ ) [20,39]. In TNAP deficient cells,  $P_i$  levels should decrease while  $PP_i$  levels increase. To distinguish between  $P_i$  and  $PP_i$  effects on ISS hypertrophic zone chondrocyte apoptosis, we next isolated the ISS from wild type mice and cultured them for five days in media +/-  $P_i$  and  $PP_i$ . Treatment with  $P_i$  increased resting zone and proliferating zone widths, which is not entirely surprising considering that  $P_i$  is a known mitogen [18]. We were surprised to find that culture with  $P_i$  increased ISS hypertrophic zone widths because, as stated above,  $P_i$  was previously shown to be essential for promoting hypertrophic chondrocyte apoptosis in mice. Treatment with  $PP_i$  increased the hypertrophic chondrocyte width and decreased apoptosis, demonstrating that high  $PP_i$  levels downstream of TNAP deficiency [8,47] potentially caused the increased ISS hypertrophic zone widths seen in the *Alpl<sup>fl/fl</sup>;P0-Cre<sup>+</sup>* mice.

We next examined expression of IHH and PTHrP upon treatment +/-  $P_i$  and  $PP_i$ . We found that  $P_i$  but not  $PP_i$  increased expression of IHH. Treatment with  $P_i$  also increased expression of PTHrP, but  $PP_i$  did so to a much greater extent. Because  $P_i$  levels are anticipated to be low in TNAP deficient cells and tissues, this data again supports a hypothesis that high  $PP_i$  levels mediate some of the abnormal ISS development seen in *Alpl<sup>fl/fl</sup>;P0-Cre<sup>+</sup>* as compared to control mice. We also found that  $P_i$  increased while  $PP_i$  decreased Col X and Sox9 expression which is not consistent with the idea that decreased  $P_i$  or increased  $PP_i$  downstream of TNAP deficiency in *Alpl<sup>fl/fl</sup>;P0-Cre<sup>+</sup>* ISS mediated the increase Col X and Sox9 expression found in vivo. The differences seen between organ culture and in vivo immunofluorescent expression of IHH, PTHrP, Col X and Sox9 could be explained by the absence of factors that may mediate downstream effects of  $P_i$  in organ culture that are present in vivo, and/or that we utilized newborn ISS for the organ culture studies.

To establish effects of TNAP deficiency on earlier lineage neural crest cells, we transduced the O9.1 neural crest cell line with TNAP or control nontarget shRNA. The O9-1 cell line stably expresses stem cell markers and neural crest markers, and are capable of contributing to cranial neural crest fates [26,48]. We then assessed expression of stem cell and neural crest markers in these cells. Minimal differences were seen in known markers of neural crest between the cell genotypes, other than Sox9. Sox9 is known to be essential in early neural crest cells likely for maintaining pluripotency [49] and later in establishing a chondrogenic lineage [50], plus its previously discussed ability to control the proliferation and maturation of growth plate chondrocytes [51]. Lower Sox9 expression in the O9.1 cells could be an artifact of in vitro experimentation or indicate that TNAP deficiency in pluripotent cranial neural crest cells has dual effects, one earlier in development that lowers the tendency for initial chondrocyte fate commitment and one later in development (studied here) for altering growth plate chondrocyte maturation. Suppression of TNAP by shRNA decreased expression of stem cell markers Nestin and Sca1 but increased expression of CD44. Future studies are needed to establish a role for TNAP in neural crest chondrocyte lineage specification.

Overall, our results validate that TNAP expression is required in cranial neural crest cells for normal anterior cranial base development, but not for craniosynostosis. TNAP deficiency in the intersphenoid synchondrosis (ISS) leads to aberrant Sox9 and IHH-PTHrP signaling; with increased proliferation, abnormal chondrocyte maturation and diminished apoptosis. Cranial base organ culture experiments appear to demonstrate that the apoptotic abnormalities are also mediated at least in part by increased levels of  $PP_i$  that occur downstream of TNAP deficiency.

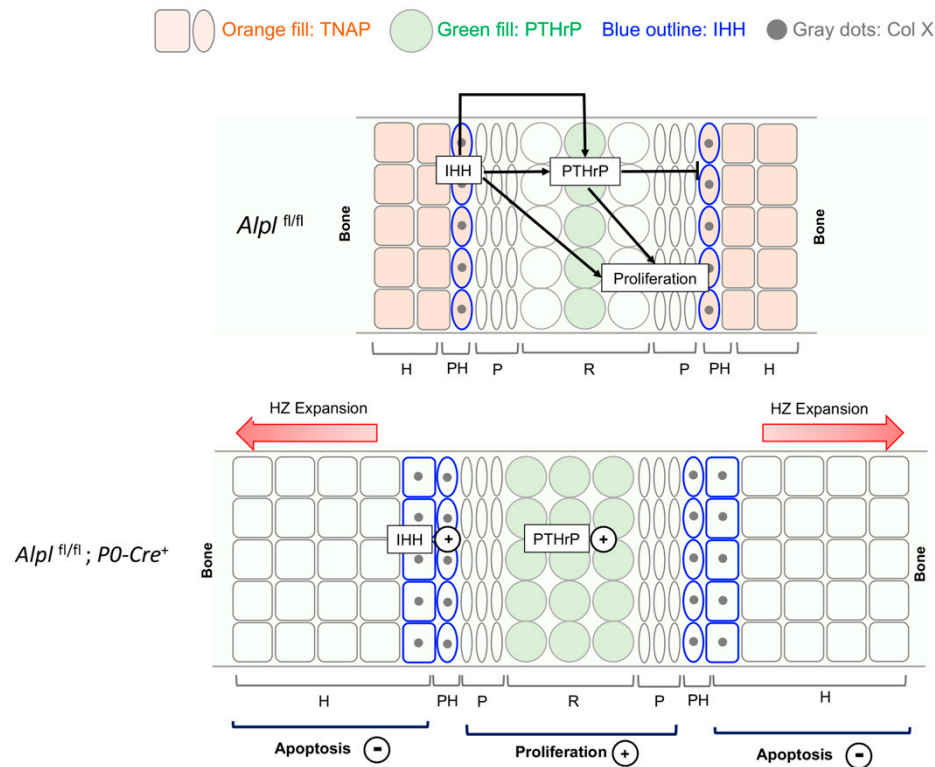


**Figure 8. Model depicting the major changes caused by conditional *Alpl* deletion in cranial base development.** The intersphenoidal synchondrosis (ISS) is a cranial base growth plate that grows in an analogous fashion to long bone growth plates, but is bidirectional in anatomy and function. The IHH-PTHrP signaling loop is essential for control of chondrocyte proliferation and maturation. IHH is expressed primarily in prehypertrophic chondrocytes where PTHrP is low. IHH acts to promote chondrocyte proliferation and chondrocyte maturation, while also stimulating PTHrP expression. PTHrP acts on resting zone chondrocytes to maintain chondrocyte proliferation and inhibit differentiation/maturation. In control mice, TNAP is expressed in prehypertrophic zone and hypertrophic zone cells. Ablation of TNAP increases both IHH and PTHrP expression. Ablation of TNAP also increases proliferation, increases ColX expression and diminishes apoptosis leading to hypertrophic zone expansion. While not shown here, ablation of TNAP via cranial neural crest P0-Cre also increases expression of Sox9 in both resting and prehypertrophic chondrocytes. Sox9 is a master transcriptional regulator that promotes chondrocyte proliferation and inhibits maturation in resting and proliferating zones, while promoting maturation and hypertrophy in prehypertrophic zones, via differential expression of co-transcription factors. Because TNAP is co-expressed with Sox9 and with IHH in control mice, we hypothesize that TNAP ablation increases chondrocyte proliferation, increases ColX expression and diminishes apoptosis through increased Sox9 expression and/or increased IHH expression (IHH in turn would increase PTHrP expression). Increased levels of inorganic pyrophosphate (PP<sub>i</sub>) may also contribute to the diminished apoptosis and hypertrophic zone expansion in TNAP deficient mice, as this effect was strongly seen in the ISS organ culture studies.

## 4. Materials and Methods

### 4.1. Animals

Mice carrying Cre recombinase driven by the protein zero (P0) promoter (*P0-Cre* mouse, C57BL/6J-*Tg(P0-Cre)*<sup>94Imeg</sup>) were generously provided by Yuji Mishina (University of Michigan, School of Dentistry, Ann Arbor, MI, USA). Floxed *Alpl* (*Alpl*<sup>fl/+</sup>) were generously provided by José Luis Millán (Sanford Children's Health Research Center, Human Genetics Program, La Jolla, CA, USA). *Alpl*<sup>fl/+</sup> and *P0-Cre* mice were bred onto a 97% 129/SvJ (Jackson Laboratory, Bar Harbor, ME,

USA) and 3% C57BL/6J (Charles River Laboratory, Wilmington, MA, USA) genetic background for a minimum of 7 generations prior to breeding for experimentation. *P0-Cre* transgenic mice were bred with *Alpl<sup>fl/+</sup>* mice to generate *Alpl<sup>fl/+</sup>; P0-Cre<sup>+</sup>* mice, which were then bred with *Alpl<sup>fl/fl</sup>* mice to generate *Alpl<sup>fl/fl</sup>; P0-Cre<sup>+</sup>*, *Alpl<sup>fl/fl</sup>* and *Alpl<sup>fl/+</sup>* mice. Litter-matched *Alpl<sup>fl/fl</sup>; P0-Cre<sup>+</sup>* (experimental mice) and *Alpl<sup>fl/fl</sup>* (control mice) were used in this study. The genotyping of the mice was determined by the following specific primers using tail DNA. Primer A (5'-TTG CGA TGT GTG AAG ATG TCC-3') and B (5'-GGC TTG CTG TCG CCA GTA AC-3') were used to detect the floxed allele (expected size: wild type band is 224 bp, floxed band is 258 bp). Primer C (5'-ATG GTG TTG CCG CGC CAT CTG CCA-3') and D (5'-CTA ATC GCC ATC TTC CAG CAG GCG-3') were used to detect the Cre-recombined allele (expected size: 298 bp). Animals were maintained and used in compliance with institutional animal care protocols of the University of Michigan's University Committee on Use and Care of Animals, and in accordance with federal guidelines for and use and care of animals in research. Because all the transgenic animals remained healthy and viable, no animals were excluded from the study. The experimental unit for in vivo studies was one mouse. Sample sizes for postnatal day 5 analyses were n=6. Sample sizes for postnatal day 35 analyses were n=20. The larger sample size used in day 35 analyses was based upon prior data generated by our lab which indicated need for this large of a sample size to reach statistical conclusions regarding craniosynostosis and cranial base fusions, due to phenotype severity variability seen in *Alpl<sup>-/-</sup>* mice. Mouse genotype was blinded for analyses then re-identified for statistical comparisons. Primary endpoints were to confirm knockout of TNAP in cranial neural crest but not paraxial mesoderm derived skull tissues (eg: the ISS but not the SOS), incidence of craniosynostosis and incidence cranial base fusions. Secondary endpoints were analyses of cranial base zones, as well as chondrocyte signaling, proliferation, differentiation and apoptosis.

#### 4.2. Nano Computed Tomography

Whole skulls of 35-day-old *Alpl<sup>fl/fl</sup>; P0-Cre<sup>+</sup>* and *Alpl<sup>fl/fl</sup>* mice were collected, fixed in 4% paraformaldehyde, serially dehydrated and stored in 70% ethanol at 4°C until scan. Whole skull specimens were scanned at 80 kV and 400  $\mu$ A with a 0.381 mm aluminum filter in a Nanotom M scanner (Waygate Technologies LP, Pasadena, Texas). In total, 1500 projection images were acquired at a source-to-axis distance of 48 mm for a resolution of 12  $\mu$ m/voxel. Three-dimensional reconstructed nano-CT images were analyzed using Dragonfly image analysis software (Version 2021.1.0.977; Object Research Systems, Inc, Montreal Canada). No significant difference between genders was found; therefore, genders were combined for analyses (n = 20 per *Alpl<sup>fl/fl</sup>; P0-Cre<sup>+</sup>* and *Alpl<sup>fl/fl</sup>* mice).

#### 4.3. Linear Skull and Cranial Base Measurements

Linear craniofacial measurements between landmarks were calculated using an electronic digital caliper (Automation and Metrology Inc., Mentor, OH, USA) on whole dissected skulls. Linear skull and cranial base measurements were performed using previously defined skull landmarks [13,52,53] (Supplemental Figure S1). Measurements were performed twice for each measurement with the average used as a given measurement per mouse. The measurements included standard craniofacial measurements used by the Craniofacial Mutant Mouse Resource of Jackson Laboratory (Bar Harbor, ME USA), which are nasal bone length (landmark 1-2), nose length (landmark 1-3), inner canthal distance (landmark 8-9), skull width (landmark 5-6), skull length (landmark 1-7), frontal bone length (landmark 2-3), and parietal bone length (landmark 3-4). The Jackson Laboratory skull height measurement was substituted with a cranial height measurement taken between pari (landmark 4) and the inferior portion of the spheno-occipital synchondrosis (landmark 10), due to the elimination of the mandible in our study.

#### 4.4. Histology and Histomorphometry

Whole skulls were dissected from *Alpl<sup>fl/fl</sup>; P0-Cre<sup>+</sup>* and *Alpl<sup>fl/fl</sup>* mice at postnatal 0 and 5 days. The skulls were fixed in the 4% paraformaldehyde (PFA) for 24 hours. The specimens were cryoprotected

in 30% sucrose in 0.01 mol/L PBS, embedded in an embedding medium (O. C. T. compound, Fisher Healthcare, USA), frozen on dry ice, and kept at -80°C until sectioning. Serial sagittal sections were cut at thickness of 14 µm and processed for H&E (hematoxylin and eosin) staining, alcian blue staining, alkaline phosphatase (ALP) staining or immunofluorescence. Zone area, zone fraction and cell number in synchondrosis were analyzed using Image J software (version 1.50i).

For alcian blue staining, the specimens were brought to room temperature (RT), then fixed by 4% PFA for 15 min, washed in PBS 5 min × 3 times, treated with 3% acetic acid for 5 min then Alcian blue 8GX (Sigma-Aldrich) for 10 min, then counterstained with nuclear fast red. For ALP activity staining, the specimens were brought to room temperature, then washed in acetone for 15 min, TBST (Tris-buffered saline pH 8.0, 1% Tween-20) for 60 min, then NTMT (0.1 M NaCl, 0.1 M Tris-HCl pH 9.5, 50 mM MgCl<sub>2</sub>, 0.1% Tween-20) for 60 min at 4°C, and stained with nitro-blue tetrazolium chloride (NBT) and bromo-4-chloro-3'-indolylphosphate *p*-toluidine (BCIP) at room temperature for 10 min, then counterstained with nuclear fast red.

#### 4.5. Immunofluorescence

Primary antibodies and their corresponding antigen retrieval methods are shown in Table 1. Sections were postfixed in 4% PFA for 10 minutes at room temperature. For immunostaining, sections were permeabilized with 0.3M glycine/0.25% Triton X/PBS for 60min, blocked with 5% skim milk/10% goat serum/ 0.05% Triton X/PBS for 60 minutes, and incubated with each antibody overnight at 4°C, and subsequently with goat anti-rabbit IgG antibody-conjugated Alexa Fluor 555 (1:400, Invitrogen) with 4'-diamidino-2-phenylindole dihydrochloride (DAPI; ProLong Gold antifade reagent, Invitrogen) staining for the nucleus. Apoptotic cells were detected using TUNEL-based in situ cell death detection kit (Invitrogen) according to the product's procedure. We performed the quantification of TUNEL by counting all TUNEL+ cells relative to the total area of the anterior and/or posterior hypertrophic zones of the ISS or SOS. Immunofluorescence negative controls were performed by replacing the primary antibody with PBS: these showed no specific immunoreaction (data not shown). Digital images were taken using a Nikon Eclipse E800 microscope with attached CCD camera. To create dual-color images, the images of the same field obtained with fluorochrome were merged using image-processing software (Affinity Photo).

**Table 1.** Primary Antibodies.

Antibody	Company	Cat. #	Type	Anti-retrieval	Dilution
Ki67	Abcam	ab16667	Rabbit Monoclonal	0.5% Trypsin 37°C 20min	200
PTHrP	Invitrogen (Thermo Fisher Scientific)	PA5-102455	Rabbit Polyclonal	No	500
IHH	Abcam	ab39634	Rabbit Polyclonal	No	100
Col 2	Abcam	ab34712	Rabbit Polyclonal	pH6.0 5.5mM Citric Acid 90°C 20min, RT 20min	100
Col X	Cosmo Bio USA	LSL-LB-0092	Rabbit Polyclonal	No	100
Sox9	Abcam	ab185966	Rabbit Monoclonal	No	500



#### 4.6. O9.1 Cell Culture and Procedures

O9-1 cells (neural crest cell line) were cultured in basal media containing DMEM (Gibco), 15% fetal bovine serum (FBS), 0.1mM non-essential amino acids (Gibco), 2mM L-glutamine (Gibco), 55 $\mu$ M beta-mercaptoethanol (Gibco), 1mM sodium pyruvate (Gibco), 100 U/mL penicillin and 100  $\mu$ g/mL streptomycin (Gibco) that had been conditioned by SNL feeder cells (ATCC, Manassas, VA, USA) overnight. The media was filtered (0.22- $\mu$ m pore size) and supplemented with 25 ng/mL basic fibroblast growth factor (bFGF; R&D Systems, Minneapolis, MN, USA) and 1,000U/mL leukemia inhibitory factor (LIF; Millipore, Burlington, MA, USA).

O9-1 cells were expanded on a fibronectin (Sigma-Aldrich)-coated plate. O9-1 cells were seeded at 10,000-15,000 cells/cm<sup>2</sup>, followed by 3 days of culture to reach confluence for freezing or plating for experimentation. To induce chondrocyte differentiation, monolayer culture was initially cultured in early differentiation media ( $\alpha$ -minimum essential medium (MEM), 10% FBS, 100U/mL penicillin, 100  $\mu$ g/mL streptomycin, 0.1mM dexamethasone, 5mM NaPO<sub>4</sub>, 50  $\mu$ g/mL ascorbic acid, and 100ng/mL BMP2 (R&D Systems) for 3 days. Then, cells were trypsinized and cultured in a micromass format in a chondrogenic medium ( $\alpha$ -MEM, 5% FBS, 1% ITS; Sigma-Aldrich Burlington, MA, USA), 100U/mL penicillin, 100  $\mu$ g/mL streptomycin, 10 ng/mL TGF- $\beta$ 3 (R&D Systems), 50  $\mu$ g/mL ascorbic acid, 10 ng/mL BMP2, 0.1 $\mu$ M dexamethasone, and 1mM sodium pyruvate] for an additional 7 days.

Alkaline phosphatase enzyme activity was assayed using the colorimetric substrate, NBT/ BCIP (Sigma-Aldrich). For alcian blue staining, cells were washed with phosphate buffered saline, fixed with 10% formalin, then stained with a 1% alcian blue solution (1% alcian blue in 60% ethanol/40% acetic acid). After destaining in 60% ethanol/40% acetic acid, cells were photographed with microscope, and each well was scanned. Scanned wells (n=3 per genotype) were quantified by densitometry using Image J software.

#### 4.7. RNA Analysis

For RNA analysis, RNA was isolated using Trizol reagent (Invitrogen, Carlsbad, CA) following manufacturer protocols. mRNA levels were assayed by reverse transcription and real time PCR. Real time PCR was performed utilizing the murine *Gapdh* primer/probe set Mm99999915\_g1, the murine *Alpl* primer/probe set Mm00475834\_m1, the murine *Sox9* primer/probe set Mm00448840\_m1, the murine *AP-2 $\alpha$*  primer/probe set Mm00495574\_m1, the murine *Twist1* primer/probe set Mm00442036\_m1, the murine *Snail1* primer/probe set Mm00441533\_m1 (neural crest cell markers), the murine *Nestin* primer/probe set Mm00450205\_m1, the murine primer/probe set *CD44* Mm01277163\_m1, the murine *Sca1* primer/probe set Mm00618853\_m1 (Stem cell markers), and Taqman Universal PCR Master Mix (Applied Biosystems, Waltham MA, USA). Real-time PCR was performed on a ViiA7 thermocycler (Life Technologies, Carlsbad, CA) and quantified by comparison to standard curve. Results are presented as normalized to *Gapdh* mRNA levels.

#### 4.8. Organ Culture and Procedures

Cranial baes structures were dissected at birth from mice and cultured in 12-well plates. Cultures were submerged in 1mL Dulbecco's modified Eagle (-) medium (DMEM, Gibco, Billings, MT, USA), containing with 100  $\mu$ g/mL Ascorbic acid, 2mg/ml insulin/transferrin/selenium (ITS, Sigma-Aldrich), 100 U/mL Penicillin G and 100  $\mu$ g/mL streptomycin (Gibco), and amphotericin B (Gibco). Experimental cultures were exposed to sodium Pi at 1 mM, or sodium PPi at 0.5mM, or without PPi/Pi. Medium was changed every two days.

#### 4.9. Statistical Analyses

All quantified data are presented as means  $\pm$  standard deviations. Statistical analyses were performed using GraphPad Prism (GraphPad Software Inc., San Diego, CA, USA). The student's t-test was applied for two-group comparisons and the ANOVA was used for multiple-group comparisons. Fishers exact test was used to analyze the incidence of ISS fusion in 35-day-old mice. A p-value of < 0.05 was considered statistically significant.

## 5. Conclusions

### Supplementary Materials:

**Author Contributions:** Conceptualization, N.H. and N.O.; methodology, N.H., N.O. and H.N.; formal analysis, N.O. and N.H.; investigation, N.O., H.N.; resources, N.H.; writing—original draft preparation, N.O. and N.H.; writing—review and editing, N.H., N.O. F.L., H.N.; supervision, N.H. and H.N.; project administration, N.H.; funding acquisition, N.H. All authors have read and agreed to the published version of the manuscript.

**Funding:** This research was funded by the National Institute of Dental and Craniofacial Research, grant number R01 DE025827.

**Institutional Review Board Statement:** This study was conducted in accordance with the Declaration of Helsinki, and approved by the Institutional Review Board of the University of Michigan, University of Michigan's University Committee on Use and Care of Animals (protocol PRO00010590, approved 12/14/2021).

**Data Availability Statement:** the data presented in this study are available on request from the corresponding author.

**Conflicts of Interest:** The authors declare no conflict of interest.

### References:

1. Abad, V.; Meyers, J. L.; Weise, M.; Gafni, R. I.; Barnes, K. M.; Nilsson, O.; Bacher, J. D.; Baron, J., The role of the resting zone in growth plate chondrogenesis. *Endocrinology* **2002**, *143*, (5), 1851-7.
2. Kronenberg, H. M., Developmental regulation of the growth plate. *Nature* **2003**, *423*, (6937), 332-6.
3. Nie, X., Cranial base in craniofacial development: developmental features, influence on facial growth, anomaly, and molecular basis. *Acta Odontol Scand* **2005**, *63*, (3), 127-35.
4. Funato, N., New Insights Into Cranial Synchronosis Development: A Mini Review. *Front Cell Dev Biol* **2020**, *8*, 706.
5. Hessle, L.; Johnson, K. A.; Anderson, H. C.; Narisawa, S.; Sali, A.; Goding, J. W.; Terkeltaub, R.; Millan, J. L., Tissue-nonspecific alkaline phosphatase and plasma cell membrane glycoprotein-1 are central antagonistic regulators of bone mineralization. *Proc Natl Acad Sci U S A* **2002**, *99*, (14), 9445-9.
6. Murshed, M.; Harmey, D.; Millan, J. L.; McKee, M. D.; Karsenty, G., Unique coexpression in osteoblasts of broadly expressed genes accounts for the spatial restriction of ECM mineralization to bone. *Genes Dev* **2005**, *19*, (9), 1093-104.
7. Narisawa, S.; Frohlander, N.; Millan, J. L., Inactivation of two mouse alkaline phosphatase genes and establishment of a model of infantile hypophosphatasia. *Dev Dyn* **1997**, *208*, (3), 432-46.
8. Fedde, K. N.; Blair, L.; Silverstein, J.; Coburn, S. P.; Ryan, L. M.; Weinstein, R. S.; Waymire, K.; Narisawa, S.; Millan, J. L.; MacGregor, G. R.; Whyte, M. P., Alkaline phosphatase knock-out mice recapitulate the metabolic and skeletal defects of infantile hypophosphatasia. *J Bone Miner Res* **1999**, *14*, (12), 2015-26.
9. Whyte, M. P.; Zhang, F.; Wenkert, D.; McAlister, W. H.; Mack, K. E.; Benigno, M. C.; Coburn, S. P.; Wagy, S.; Griffin, D. M.; Ericson, K. L.; Mumm, S., Hypophosphatasia: validation and expansion of the clinical nosology for children from 25 years experience with 173 pediatric patients. *Bone* **2015**, *75*, 229-39.
10. Whyte, M. P., Hypophosphatasia - aetiology, nosology, pathogenesis, diagnosis and treatment. *Nat Rev Endocrinol* **2016**, *12*, (4), 233-46.
11. Collmann, H.; Mornet, E.; Gattenlohner, S.; Beck, C.; Girschick, H., Neurosurgical aspects of childhood hypophosphatasia. *Childs Nerv Syst* **2009**, *25*, (2), 217-23.
12. Liu, J.; Nam, H. K.; Campbell, C.; Gasque, K. C.; Millan, J. L.; Hatch, N. E., Tissue-nonspecific alkaline phosphatase deficiency causes abnormal craniofacial bone development in the *Alpl*(-/-) mouse model of infantile hypophosphatasia. *Bone* **2014**, *67*, 81-94.
13. Nam, H. K.; Sharma, M.; Liu, J.; Hatch, N. E., Tissue Nonspecific Alkaline Phosphatase (TNAP) Regulates Cranial Base Growth and Synchronosis Maturation. *Front Physiol* **2017**, *8*, 161.
14. Chen, G.; Ishan, M.; Yang, J.; Kishigami, S.; Fukuda, T.; Scott, G.; Ray, M. K.; Sun, C.; Chen, S. Y.; Komatsu, Y.; Mishina, Y.; Liu, H. X., Specific and spatial labeling of P0-Cre versus Wnt1-Cre in cranial neural crest in early mouse embryos. *Genesis* **2017**, *55*, (6).
15. St-Jacques, B.; Hammerschmidt, M.; McMahon, A. P., Indian hedgehog signaling regulates proliferation and differentiation of chondrocytes and is essential for bone formation. *Genes Dev* **1999**, *13*, (16), 2072-86.
16. Wei, X.; Hu, M.; Mishina, Y.; Liu, F., Developmental Regulation of the Growth Plate and Cranial Synchronosis. *J Dent Res* **2016**, *95*, (11), 1221-9.
17. Beck, G. R., Jr.; Moran, E.; Knecht, N., Inorganic phosphate regulates multiple genes during osteoblast differentiation, including *Nrf2*. *Exp Cell Res* **2003**, *288*, (2), 288-300.

18. Camalier, C. E.; Yi, M.; Yu, L. R.; Hood, B. L.; Conrads, K. A.; Lee, Y. J.; Lin, Y.; Garneys, L. M.; Bouloux, G. F.; Young, M. R.; Veenstra, T. D.; Stephens, R. M.; Colburn, N. H.; Conrads, T. P.; Beck, G. R., Jr., An integrated understanding of the physiological response to elevated extracellular phosphate. *J Cell Physiol* **2013**, 228, (7), 1536-50.
19. Nam, H. K.; Liu, J.; Li, Y.; Kragor, A.; Hatch, N. E., Ectonucleotide pyrophosphatase/phosphodiesterase-1 (ENPP1) protein regulates osteoblast differentiation. *J Biol Chem* **2011**, 286, (45), 39059-71.
20. Kim, H. J.; Delaney, J. D.; Kirsch, T., The role of pyrophosphate/phosphate homeostasis in terminal differentiation and apoptosis of growth plate chondrocytes. *Bone* **2010**, 47, (3), 657-65.
21. McElwee, K. J.; Kissling, S.; Wenzel, E.; Huth, A.; Hoffmann, R., Cultured peribulbar dermal sheath cells can induce hair follicle development and contribute to the dermal sheath and dermal papilla. *J Invest Dermatol* **2003**, 121, (6), 1267-75.
22. Kermer, V.; Ritter, M.; Albuquerque, B.; Leib, C.; Stanke, M.; Zimmermann, H., Knockdown of tissue nonspecific alkaline phosphatase impairs neural stem cell proliferation and differentiation. *Neurosci Lett* **2010**, 485, (3), 208-11.
23. Yasuda, S. Y.; Tsuneyoshi, N.; Sumi, T.; Hasegawa, K.; Tada, T.; Nakatsuji, N.; Suemori, H., NANOG maintains self-renewal of primate ES cells in the absence of a feeder layer. *Genes Cells* **2006**, 11, (9), 1115-23.
24. O'Connor, M. D.; Kardel, M. D.; Iosifina, I.; Youssef, D.; Lu, M.; Li, M. M.; Vercauteren, S.; Nagy, A.; Eaves, C. J., Alkaline phosphatase-positive colony formation is a sensitive, specific, and quantitative indicator of undifferentiated human embryonic stem cells. *Stem Cells* **2008**, 26, (5), 1109-16.
25. Brambrink, T.; Foreman, R.; Welstead, G. G.; Lengner, C. J.; Wernig, M.; Suh, H.; Jaenisch, R., Sequential expression of pluripotency markers during direct reprogramming of mouse somatic cells. *Cell Stem Cell* **2008**, 2, (2), 151-9.
26. Nguyen, B. H.; Ishii, M.; Maxson, R. E.; Wang, J., Culturing and Manipulation of O9-1 Neural Crest Cells. *J Vis Exp* **2018**, (140).
27. Whyte, M. P.; Greenberg, C. R.; Salman, N. J.; Bober, M. B.; McAlister, W. H.; Wenkert, D.; Van Sickle, B. J.; Simmons, J. H.; Edgar, T. S.; Bauer, M. L.; Hamdan, M. A.; Bishop, N.; Lutz, R. E.; McGinn, M.; Craig, S.; Moore, J. N.; Taylor, J. W.; Cleveland, R. H.; Cranley, W. R.; Lim, R.; Thacher, T. D.; Mayhew, J. E.; Downs, M.; Millan, J. L.; Skrinar, A. M.; Crine, P.; Landy, H., Enzyme-replacement therapy in life-threatening hypophosphatasia. *N Engl J Med* **2012**, 366, (10), 904-13.
28. Fraser, D., Hypophosphatasia. *Am J Med* **1957**, 22, (5), 730-46.
29. Mishina, Y.; Snider, T. N., Neural crest cell signaling pathways critical to cranial bone development and pathology. *Exp Cell Res* **2014**, 325, (2), 138-47.
30. Jiang, X.; Iseki, S.; Maxson, R. E.; Sucov, H. M.; Morriss-Kay, G. M., Tissue origins and interactions in the mammalian skull vault. *Dev Biol* **2002**, 241, (1), 106-16.
31. Yoshida, T.; Vivatbutsiri, P.; Morriss-Kay, G.; Saga, Y.; Iseki, S., Cell lineage in mammalian craniofacial mesenchyme. *Mech Dev* **2008**, 125, (9-10), 797-808.
32. Deckelbaum, R. A.; Holmes, G.; Zhao, Z.; Tong, C.; Basilico, C.; Loomis, C. A., Regulation of cranial morphogenesis and cell fate at the neural crest-mesoderm boundary by engrailed 1. *Development* **2012**, 139, (7), 1346-58.
33. Vora, S. R.; Camci, E. D.; Cox, T. C., Postnatal Ontogeny of the Cranial Base and Craniofacial Skeleton in Male C57BL/6J Mice: A Reference Standard for Quantitative Analysis. *Front Physiol* **2015**, 6, 417.
34. Nam, H. K.; Vesela, I.; Siismets, E.; Hatch, N. E., Tissue nonspecific alkaline phosphatase promotes calvarial progenitor cell cycle progression and cytokinesis via Erk1,2. *Bone* **2018**, 120, 125-136.
35. Nam, H. K.; Emmanouil, E.; Hatch, N. E., Deletion of the Pyrophosphate Generating Enzyme ENPP1 Rescues Craniofacial Abnormalities in the TNAP(-/-) Mouse Model of Hypophosphatasia and Reveals FGF23 as a Marker of Phenotype Severity. *Front Dent Med* **2022**, 3.
36. Ishii, M.; Merrill, A. E.; Chan, Y. S.; Gitelman, I.; Rice, D. P.; Sucov, H. M.; Maxson, R. E., Jr., Msx2 and Twist cooperatively control the development of the neural crest-derived skeletogenic mesenchyme of the murine skull vault. *Development* **2003**, 130, (24), 6131-42.
37. Sun, J.; Ishii, M.; Ting, M. C.; Maxson, R., Foxc1 controls the growth of the murine frontal bone rudiment by direct regulation of a Bmp response threshold of Msx2. *Development* **2013**, 140, (5), 1034-44.
38. Kaufman, M. H., *The Atlas of Mouse Development*. Amsterdam, Boston, London, New York: The Elsevier Academic Press.: 2003.
39. Sabbagh, Y.; Carpenter, T. O.; Demay, M. B., Hypophosphatemia leads to rickets by impairing caspase-mediated apoptosis of hypertrophic chondrocytes. *Proc Natl Acad Sci U S A* **2005**, 102, (27), 9637-42.
40. Leung, V. Y.; Gao, B.; Leung, K. K.; Melhado, I. G.; Wynn, S. L.; Au, T. Y.; Dung, N. W.; Lau, J. Y.; Mak, A. C.; Chan, D.; Cheah, K. S., SOX9 governs differentiation stage-specific gene expression in growth plate chondrocytes via direct concomitant transactivation and repression. *PLoS Genet* **2011**, 7, (11), e1002356.
41. Dy, P.; Wang, W.; Bhattaram, P.; Wang, Q.; Wang, L.; Ballock, R. T.; Lefebvre, V., Sox9 directs hypertrophic maturation and blocks osteoblast differentiation of growth plate chondrocytes. *Dev Cell* **2012**, 22, (3), 597-609.

42. Akiyama, H.; Chaboissier, M. C.; Martin, J. F.; Schedl, A.; de Crombrughe, B., The transcription factor Sox9 has essential roles in successive steps of the chondrocyte differentiation pathway and is required for expression of Sox5 and Sox6. *Genes Dev* **2002**, 16, (21), 2813-28.
43. Vortkamp, A.; Lee, K.; Lanske, B.; Segre, G. V.; Kronenberg, H. M.; Tabin, C. J., Regulation of rate of cartilage differentiation by Indian hedgehog and PTH-related protein. *Science* **1996**, 273, (5275), 613-22.
44. Lanske, B.; Karaplis, A. C.; Lee, K.; Luz, A.; Vortkamp, A.; Pirro, A.; Karperien, M.; Defize, L. H.; Ho, C.; Mulligan, R. C.; Abou-Samra, A. B.; Juppner, H.; Segre, G. V.; Kronenberg, H. M., PTH/PTHrP receptor in early development and Indian hedgehog-regulated bone growth. *Science* **1996**, 273, (5275), 663-6.
45. Nie, X.; Luukko, K.; Kvinnsland, I. H.; Kettunen, P., Developmentally regulated expression of Shh and Ihh in the developing mouse cranial base: comparison with Sox9 expression. *Anat Rec A Discov Mol Cell Evol Biol* **2005**, 286, (2), 891-8.
46. Hallett, S. A.; Ono, W.; Franceschi, R. T.; Ono, N., Cranial Base Synchronosis: Chondrocytes at the Hub. *Int J Mol Sci* **2022**, 23, (14).
47. Nam, H. K.; Emmanouil, E.; Hatch, N. E., Deletion of the Pyrophosphate Generating Enzyme ENPP1 Rescues Craniofacial Abnormalities in the TNAP<sup>-/-</sup> Mouse Model of Hypophosphatasia and Reveals FGF23 as a Marker of Phenotype Severity. *Frontiers in Dental Medicine* **2022**, 3.
48. Ishii, M.; Arias, A. C.; Liu, L.; Chen, Y. B.; Bronner, M. E.; Maxson, R. E., A stable cranial neural crest cell line from mouse. *Stem Cells Dev* **2012**, 21, (17), 3069-80.
49. Schock, E. N.; LaBonne, C., Sorting Sox: Diverse Roles for Sox Transcription Factors During Neural Crest and Craniofacial Development. *Front Physiol* **2020**, 11, 606889.
50. Mori-Akiyama, Y.; Akiyama, H.; Rowitch, D. H.; de Crombrughe, B., Sox9 is required for determination of the chondrogenic cell lineage in the cranial neural crest. *Proc Natl Acad Sci U S A* **2003**, 100, (16), 9360-5.
51. Chen, H.; Tan, X. N.; Hu, S.; Liu, R. Q.; Peng, L. H.; Li, Y. M.; Wu, P., Molecular Mechanisms of Chondrocyte Proliferation and Differentiation. *Front Cell Dev Biol* **2021**, 9, 664168.
52. Liu, J.; Nam, H. K.; Wang, E.; Hatch, N. E., Further analysis of the Crouzon mouse: effects of the FGFR2(C342Y) mutation are cranial bone-dependent. *Calcif Tissue Int* **2013**, 92, (5), 451-66.
53. de F, A.-S. A., Costilla S, Noval I, A. J, Cobo J, 3D-μCT Cephalometric Measurements in Mice. . *InTech* **2011**.